Continuum Mech. Thermodyn.
DOI 10.1007/s00161-013-0315-8

ORIGINAL ARTICLE

Mikhail B. Babenkov · Elena A. Ivanova

Analysis of the wave propagation processes in heat transfer problems of the hyperbolic type

Received: 20 March 2013 / Accepted: 1 August 2013
© Springer-Verlag Berlin Heidelberg 2013

Abstract A number of problems for the interaction of laser radiation with a heat-conducting half-space and a layer are considered. The obtained solutions are compared with each other and with the solutions of the classic heat equation and the wave equation. A laser impulse is modelled by defining the heat flux at the boundary for the opaque medium, or by defining the distribution of heat sources in the volume for the semitransparent medium. The power of the laser pulse depends on time as the Dirac delta function or as the Heaviside function do. It allows for the simulation of instant and continuous laser exposure on the medium. Temperature distributions are obtained by using Green's functions for a half-space and a layer with the Dirichlet and Neumann boundary conditions.

Keywords Hyperbolic heat conduction · Heat flux relaxation constant · Heat propagation speed · Heat transport in nanosystems · Heat pulse

1 Introduction

Investigation of the wave heat transfer is important for many developing technologies. Internal heat sources at the nanoscale level (the size of a modern transistor is approximately a few nanometers) cause more intensive temperature growth [1] than it is predicted by the classic theory and increase the requirements for future cooling systems [2]. Temperature effects introduce significant changes to the mechanical properties of the nanolayers [3], because the thinner the layer is, the more sensitive it becomes to temperature effects. Studies of heat wave transfer can be useful for the determination of the thermomechanical characteristics of micro- and nanoscale objects such as thin plates and rods that are used in micro- and nanoelectromechanical devices (MEMS and NEMS).

Communicated by Andreas Öchsner.

M. B. Babenkov · E. A. Ivanova
Department of Theoretical Mechanics, St. Petersburg State Polytechnical University (SPb-SPU), Politekhnicheskaja 29, 195251 Saint Petersburg, Russia

M. B. Babenkov (✉) · E. A. Ivanova
Institute for Problems in Mechanical Engineering, Russian Academy of Sciences, Bolshoy pr. 61, V.O., 199178 Saint Petersburg, Russia
E-mail: babenkov.michail@gmail.com
Tel.: +7-812-7444289

E. A. Ivanova
E-mail: elenaivanova239@post.ru
Tel.: +7-812-2909872

Published online: 11 August 2013

For heat-conducting processes of sufficiently short timescales, it is appropriate [4] to consider a model that takes into account the finite speed of heat propagation:

$$\rho C_v(\tau\ddot{T} + \dot{T}) = \lambda \Delta T \tag{1}$$

where ρ is a material density, C_v is a constant volume specific heat, τ is a heat flux relaxation constant, T is the deviation from the temperature T_0 at which the material constants were measured, dot denotes time derivative, λ is the material conductivity, Δ is the Laplace operator. The derivation of this equation is based on the law of Cattaneo–Vernotte [5,6]:

$$\tau\dot{\mathbf{h}} + \mathbf{h} = -\lambda \nabla T \tag{2}$$

where $\mathbf{h}$ is a heat flux vector, ∇ is the del operator.

The Cattaneo–Vernotte law differs from classic Fourier's law in that it includes the heat flux relaxation constant τ, the presence of which means that the heat flux does not appear or disappear instantly if the temperature gradient is loaded or unloaded [4]. The propagation speed ("c") of thermal disturbances in a heat-conducting medium depends on the value of τ: $c = \sqrt{\lambda/(\rho C_v \tau)}$. The value of the heat relaxation constant ranges from 10^{-12} to 10^{-8} s for homogeneous materials in different aggregative states [7]. If timescale of the experiment is comparable to the relaxation time value, it is recommended to use a generalized Fourier's law. Concepts and fundamentals of modern thermodynamics are discussed in [4,8–11].

It is widely known that there are other more complex models of thermal conductivity with a finite speed of thermal waves in its linear approximation [4,12]: a model with a thermal memory [13], a model [14], which takes into account the time lag of the heat flux and the temperature gradient, etc. A detailed review of thermal conductivity models is presented in [4].

Equation (1) is a special case of the telegraph equation, which describes the wave propagation with losses. Limit cases of Eq. (1) are the classic heat equation, if the term $\tau\dot{\mathbf{h}}$ can be neglected, and the wave equation, if $\tau|\dot{\mathbf{h}}| \gg |\mathbf{h}|$.

2 The heat equation of the hyperbolic type

Let us consider heat-conducting media. The energy balance equation takes the following form:

$$\rho\dot{U} = -\nabla \cdot \mathbf{h} + \rho q \tag{3}$$

where U is the density of internal energy, q is the heat input rate into the volume. The relationship between internal energy and temperature is stated as follows:

$$U = C_v T \tag{4}$$

Using the Cattaneo–Vernotte law (2), one can write the system of differential equations for the temperature and the heat flux vector [15]:

$$\begin{cases} \rho C_v \dot{T} = -\nabla \cdot \mathbf{h} + \rho q \\ \mathbf{h} + \tau\dot{\mathbf{h}} = -\lambda \nabla T \end{cases} \tag{5}$$

Initial conditions for the system (5) are given by:

$$T\big|_{t=0} = f(\mathbf{s}); \quad \mathbf{h}\big|_{t=0} = \mathbf{g}(\mathbf{s}); \tag{6}$$

where $\mathbf{s}$ is the radius vector that defines the spatial position of the points of media.

By excluding the heat flux vector from the system (5), one obtains an equation for the temperature:

$$\rho C_v(\dot{T} + \tau\ddot{T}) - \lambda \Delta T = \rho(q + \tau\dot{q}) \tag{7}$$

An additional initial condition for the first-order derivative of the temperature can be obtained from the known value of the heat flux at $t = 0$ and the first equation of the system (5). Let us formulate the initial conditions for Eq. (7):

$$\dot{T}\big|_{t=0} = -\frac{1}{\rho C_v}\nabla \cdot \mathbf{g} + \frac{1}{C_v}q; \quad T\big|_{t=0} = f(\mathbf{s}); \tag{8}$$

The initial condition for the heat flux is an alternative of the initial condition for the heating rate $\dot{T}$.

If a contact method of the temperature measurement is used, the definition of $\dot{T}$ presents some difficulties. By the means of contact method, the temperature can be recorded only after the thermodynamic equilibrium over time is achieved and the temperature becomes a constant value. There are other ways to measure the temperature. One of them is a laser thermometry. It allows measuring of the temperature and the heat flux on a surface and in a volume of a sample without the contact. This method allows the observation of nonequilibrium processes of the heat transfer due to the high time resolution on the order of 10^{-12} s and the resolution by coordinate on the order of 10^{-3} m. The temperature resolution is about 0.3 °C [16,17].

Let us specify the temperature at the boundary $\partial\Omega$:

$$T\big|_{\partial\Omega} = \varphi(t, \mathbf{s}); \qquad \mathbf{s} \in \partial\Omega \tag{9}$$

It is also possible to specify a projection of the heat flux vector on a normal to the boundary Ω instead of (9):

$$h_n\big|_{\partial\Omega} = \psi(t, \mathbf{s}); \qquad \mathbf{s} \in \partial\Omega \tag{10}$$

where $h_n = \mathbf{n} \cdot \mathbf{h}$ is a projection of the heat flux vector $\mathbf{h}$ on a normal $\mathbf{n}$ to $\partial\Omega$. When the boundary conditions are imposed on the heat flux, as in the above case, it may be easier to first find $\mathbf{h}(\mathbf{s}, t)$, excluding the temperature from system (5). An equation for the vector of heat flux similar to (7) will be obtained:

$$\rho C_v(\dot{\mathbf{h}} + \tau\ddot{\mathbf{h}}) - \lambda\nabla\nabla \cdot \mathbf{h} = \lambda\rho\nabla q \tag{11}$$

An additional initial condition for $\dot{\mathbf{h}}$ can be obtained using the second equation of system (5). Let us write out the initial conditions for Eq. (11):

$$\dot{\mathbf{h}}\big|_{t=0} = -\frac{\lambda}{\tau}\nabla f - \frac{1}{\tau}\mathbf{g}; \quad \mathbf{h}\big|_{t=0} = \mathbf{g}(\mathbf{s}); \tag{12}$$

Integrating the first equation of system (5) over time, one can get the expression for the temperature:

$$T(\mathbf{s}, t) = \frac{1}{\rho C_v}\int_0^t (\rho q - \nabla \cdot \mathbf{h})\,\mathrm{d}t + f(\mathbf{s}) \tag{13}$$

If the temperature distribution was obtained using Eq. (7), one can find an expression for heat flux by solving the second equation of the system (5):

$$\mathbf{h}(\mathbf{s}, t) = \mathrm{e}^{-t/\tau}\left(\mathbf{g}(\mathbf{s}) - \frac{\lambda}{\tau}\int_0^t \mathrm{e}^{t/\tau}\nabla T(\mathbf{s}, t)\mathrm{d}t\right) \tag{14}$$

3 Wave processes in a half-space if the thermal load is applied on the boundary

Let us consider the half-space: $0 \le s \le +\infty$. External volumetric exposures are absent. The heat propagation process is described by the homogeneous heat equation. Let us introduce new variables κ and ν, which are associated with time t and the coordinate s as follows: $\kappa = s\sqrt{\rho C_v/(\lambda\tau)}$, $\nu = t/\tau$. In this case, Eq. (11) for the heat flux takes the following form:

$$\dot{h} + \ddot{h} - h'' = 0 \tag{15}$$

The prime symbols denote the derivative on κ. The value of the heat flux is limited at infinity. The heat flux is a given function of time at the boundary. The heat wave propagation process under the step and pulse boundary conditions is studied bellow.

3.1 The heat flux at the boundary depends on time as the Dirac delta function

The initial conditions for the heat flux (12) are homogeneous:

$$h\big|_{\nu=0} = 0; \quad \dot{h}\big|_{\nu=0} = 0; \tag{16}$$

The value of the heat flux at the boundary $\kappa = 0$ depends on time as the δ function:

$$h\big|_{\kappa=0} = h_0\delta(\nu - 0) \tag{17}$$

A multiplier h_0 has been added to save the heat flux dimension.

A solution of the problem (15)–(16), obtained using the Laplace transform [15,18], is given by:

$$h = h_0 \mathrm{e}^{-\nu/2}\left[\delta(\nu-\kappa) + \frac{\kappa}{2\sqrt{\nu^2-\kappa^2}} I_1\left(\frac{1}{2}\sqrt{\nu^2-\kappa^2}\right) H(\nu-\kappa)\right] \tag{18}$$

where I_1 is the modified Bessel function of the first kind. Using (13), one obtains temperature distribution in the half-space:

$$T = -\int_0^{\nu} \frac{\partial h(\kappa, \nu)}{\partial \kappa} \mathrm{d}\nu \tag{19}$$

Profiles of the temperature waves (19) are plotted at the different values of time in Fig. 1a and b.

Let us consider its two limit cases. A solution of the problem (17)–(16) for the wave equation is given by (Fig. 1c):

$$T = h_0\delta(\nu - \kappa) \tag{20}$$

For the classic heat equation, a temperature expression follows:

$$T = \frac{h_0}{\sqrt{\pi\nu}} \exp\left(-\frac{\kappa^2}{4\nu}\right) \tag{21}$$

The wave front in the solution (21) is absent. The profiles of the solution (21) for the different times are shown in Fig. 1d.

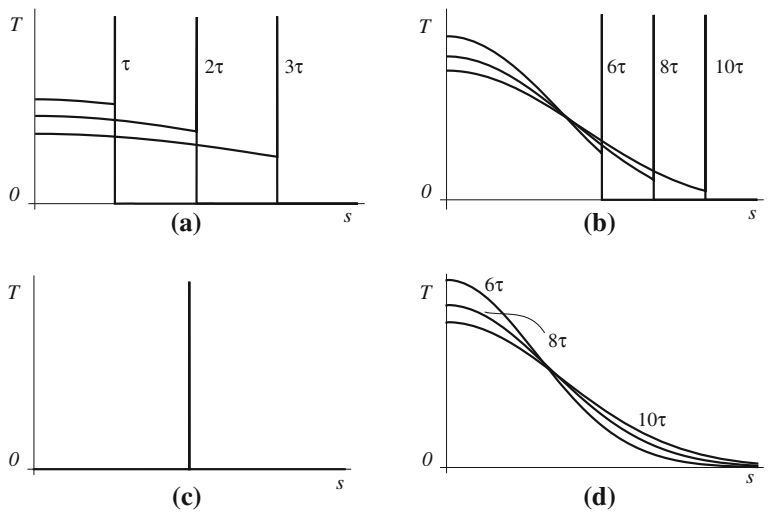

Fig. 1 Time shape of the impulse on the boundary of the half-space is the δ function. Solution profiles are plotted for the different time values: $\tau, 2\tau, 3\tau, 6\tau, 8\tau, 10\tau$ seconds; curves **a**, **b** are the solution profiles corresponding to the hyperbolic heat equation; curve **c** is the solution profile corresponding to the wave equation; curve **d** is the solution profile corresponding to the classic parabolic heat equation

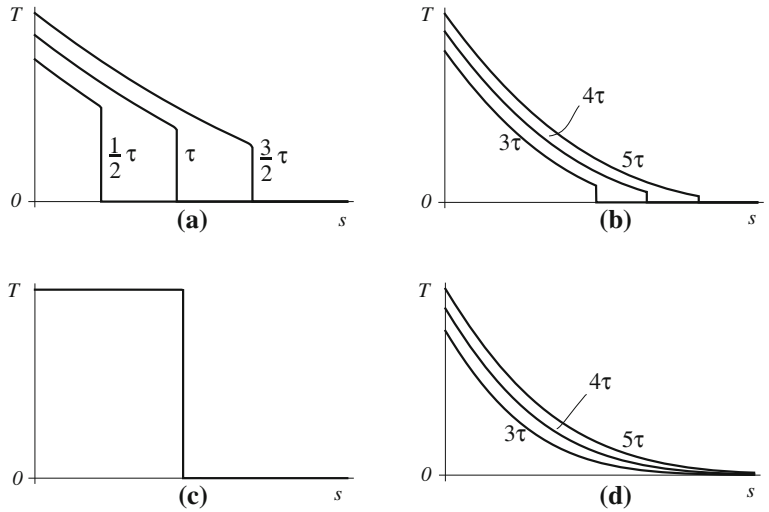

Fig. 2 Time shape of the impulse on the boundary is the Heaviside step function. Solution profiles are plotted for the different time values: $\tau/2$, τ, $3\tau/2$, 3τ, 4τ, 5τ seconds; curves **a**, **b** are the solution profiles corresponding to the hyperbolic heat equation; curve **c** is the solution profile corresponding to the wave equation; curve **d** is the solution profile corresponding to the classic parabolic heat equation

Comparing Fig. 1a and c, it is easy to see the similarities and differences between the solutions of the hyperbolic and the wave equations. The curves for both of the equations have the δ function jumps on its wave fronts. The solution of the wave equation differs from zero only at its front. The region of the wave profile of the hyperbolic equation between the origin and the wave front becomes similar to the solution of the classic heat equation with time. The differences between the solutions of the classic and hyperbolic equations become visible at the values of time of the order of the relaxation constant τ.

3.2 The heat flux at the boundary depends on time as the Heaviside step function

The value of the heat flux at the boundary depends on time as the Heaviside step function:

$$h|_{\kappa=0} = h_0\, H(\nu - 0), \qquad H(\nu) = \begin{bmatrix} 1, & \nu \geq 0 \\ 0, & \nu < 0 \end{bmatrix} \tag{22}$$

The initial conditions for the heat flux (12):

$$h\big|_{\nu=0} = 0; \quad \dot{h}\big|_{\nu=0} = 0; \tag{23}$$

A solution of the problem (15), (22), (23), obtained using the Laplace transform, is given by [19]:

$$h = h_0 \left(\exp\left(-\frac{\kappa}{2}\right) + \frac{\kappa}{2} \int_{\kappa}^{\nu} \frac{\exp\left(-\xi/2\right)}{\sqrt{\xi - \kappa^2}} I_1\left(\frac{1}{2}\sqrt{\xi - \kappa^2}\right) \mathrm{d}\xi \right) H\left(\nu - \kappa\right) \tag{24}$$

Using (19), one obtains the temperature distribution in the half-space. Profiles of the temperature waves (19) are plotted at the different values of time in Fig. 2a and b.

Let us consider the two limit cases: the wave equation and the classic heat equation. A solution of the wave equation (Fig. 2c) is given by

$$T = h_0 H\left(\nu - \kappa\right) \tag{25}$$

The classic statement of the problem leads to a following solution (in the dimensionless variables):

$$T = h_0 \left(2\exp\left(-\frac{\kappa^2}{4\nu}\right)\sqrt{\frac{\nu}{\pi}} - \mathrm{erfc}\left(\frac{\kappa}{2\sqrt{\nu}}\right)\kappa \right) \tag{26}$$

where erfc(z) is the complementary error function:

$$\operatorname{erfc}(z) = 1 - \frac{2}{\sqrt{\pi}} \int_0^z \mathrm{e}^{-\xi^2} \mathrm{d}\xi$$

A feature peculiar to the classic heat equation is the absence of the wave front in solution graphics. The graphics for the classic solution (26) are shown in Fig. 2d. For all values of time, the curves look the same, but at small values of time the temperature reaches the abscissa axis faster. Comparing Fig. 2a and c, one can see that the solution of the hyperbolic equations is similar to the solution of the wave equation for short times: the wave profile is close to a "step." The solution of the hyperbolic equation is more like the one of the parabolic equation at the larger times: the temperature discontinuity at the wave front rapidly decreases with the distance from the boundary.

4 Wave processes in the layer caused by the influence of internal heat sources

Let us consider the laser impact on the layer with the thickness of l. The penetration depth of the laser radiation into the medium can be significant at the nanoscale level even for opaque materials; thus, it is possible to use Bouguer's law for modelling the absorption of the laser radiation by the material. According to Bouguer's law, the intensity of a parallel beam of the monochromatic light exponentially decays when it passes through a medium:

$$I(s) = I_0 \mathrm{e}^{-\alpha s} \tag{27}$$

where s is the distance from the layer boundary, I_0 is the intensity of the incident light, α is an absorption coefficient of the substance. If the intensity of a short laser impulse is absorbed by the medium according to the Bouguer's law, then the power of internal sources can be written as:

$$q(s,t) = I_0 \delta(t-0) \mathrm{e}^{-\alpha s}$$

where the δ function approximates the dependence of a short laser impulse intensity on time, more precise form of which is the Gaussian distribution.

4.1 The intensity of the internal heat sources depends on time as the Dirac delta function

4.1.1 The thermally insulated layer

For the sake of brevity, let us introduce a new notation:

$$\eta = h\frac{1}{I_0}\sqrt{\frac{C_v}{\rho\lambda}}; \quad \varsigma = s\sqrt{\frac{\rho C_v}{\lambda}}; \quad \vartheta = T\frac{C_v}{I_0}; \quad \gamma = \alpha\sqrt{\frac{\lambda}{\rho C_v}}; \quad \mu = l\sqrt{\frac{\rho C_v}{\lambda}}; \tag{28}$$

The differential equation for the heat flux (11) will be represented as:

$$\dot{\eta} + \tau\ddot{\eta} - \eta'' = \gamma\delta(t-0)\mathrm{e}^{-\gamma\varsigma} \tag{29}$$

The boundary conditions for Eq. (29) are written as follows:

$$\eta\big|_{\varsigma=0} = 0; \quad \eta\big|_{\varsigma=\mu} = 0; \tag{30}$$

Initial conditions (12) for the heat flux with regard to the new notation have the form:

$$\eta\big|_{t=0} = 0; \quad \dot{\eta}\big|_{t=0} = 0; \tag{31}$$

Once obtained, the expression for $\eta(\varsigma, t)$ allows us to find the temperature distribution $\vartheta(\varsigma, t)$ for the layer if the heat flux at the boundaries is absent. For this, we use the expression (13):

$$\vartheta(\varsigma, t) = -\int_0^t \eta'(\varsigma, t)\mathrm{d}t + \mathrm{e}^{-\gamma\varsigma} H(t) \tag{32}$$

In order to obtain the solution of the problem (29)–(31), let us change the variable:

$$\eta(\varsigma, t) = \exp\left(-\frac{t}{2\tau}\right) w(\varsigma, t) \tag{33}$$

After introducing the new variable, Eq. (29) will take the form of the linear nonhomogeneous Klein–Gordon equation:

$$\ddot{w} = \frac{1}{\tau} w'' + \frac{1}{4\tau} w + \frac{\gamma}{\tau}\delta(t-0)\mathrm{e}^{-\gamma\varsigma} \tag{34}$$

The initial and boundary conditions after the variable change will have the form:

$$w\big|_{t=0} = 0; \quad \dot{w}\big|_{t=0} = 0; \quad w\big|_{\varsigma=0} = 0; \quad w\big|_{\varsigma=\mu} = 0; \tag{35}$$

The solution of (34)–(35) can be conveniently obtained by using Green's functions method. The formula [20] for the distribution of $w(\varsigma, t)$ in the layer with the homogeneous initial and boundary conditions is written as:

$$w(\varsigma, t) = \int_0^t \int_0^\mu \Phi(\xi, \zeta) G(\varsigma, \xi, t-\zeta)\mathrm{d}\xi\mathrm{d}\zeta \tag{36}$$

where Green's function G has the form [20]:

$$G(\varsigma, \xi, t) = \frac{2}{\mu}\sum_{n=1}^{\infty} \sin\left[\frac{\pi n \varsigma}{\mu}\right] \sin\left[\frac{\pi n \xi}{\mu}\right] \frac{\sin\left[t\sqrt{\frac{1}{\tau}\left(\frac{\pi n}{\mu}\right)^2 - \frac{1}{4\tau^2}}\right]}{\sqrt{\frac{1}{\tau}\left(\frac{\pi n}{\mu}\right)^2 - \frac{1}{4\tau^2}}} \tag{37}$$

The source function in Eq. (34) has a form:

$$\Phi(\varsigma, t) = \frac{\gamma}{\tau}\delta(t-0)\mathrm{e}^{-\gamma\varsigma}$$

The result of integrating expression (36) is substituted in (33) to obtain the expression for the heat flux:

$$\eta = 4\mu\gamma\, \mathrm{e}^{-\mu\gamma - \frac{1}{2}t/\tau} \sum_{n=1}^{\infty} \frac{(n\pi \mathrm{e}^{\mu\gamma} - (-1)^n) \sin\left[\frac{n\pi\varsigma}{\mu}\right] \sin\left[\frac{S_n t}{2\tau\mu}\right]}{S_n\left(n^2\pi^2 + \mu^2\gamma^2\right)} H(t) \tag{38}$$

where $S_n = \sqrt{4n^2\pi^2\tau - \mu^2}$;

It is easily seen that heat flux (38) takes the real values for any sign of the expression under the radical of S_n. Substituting (38) in (32), we obtain an expression for the temperature:

$$\begin{aligned}\vartheta = {} & \mathrm{e}^{-\varsigma\gamma} H(t) - 2\mu\gamma \mathrm{e}^{-\mu\gamma - \frac{1}{2}t/\tau} \sum_{n=1}^{\infty} \frac{\cos\left[\frac{n\pi\varsigma}{\mu}\right](\mathrm{e}^{\mu\gamma} - (-1)^n)}{S_n\left(n^2\pi^2 + \mu^2\gamma^2\right)} \\ & \times \left(S_n\left(\mathrm{e}^{\frac{t}{2\tau}} - \cos\left[\frac{S_n t}{2\mu\tau}\right]\right) - \mu \sin\left[\frac{S_n t}{2\mu\tau}\right]\right) H(t)\end{aligned} \tag{39}$$

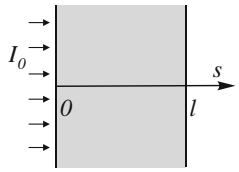

Fig. 3 The hyperbolic heat conduction problem for the semitransparent layer

A solution of the problem in the classic formulation for the insulated layer is a series obtained by Green's function method:

$$\vartheta = \frac{\mathrm{e}^{-\gamma(\varsigma - t\gamma)}}{2} \sum_{n=-\infty}^{\infty} \mathrm{e}^{-2\mu n\gamma} \left(\mathrm{erf}\left[\frac{2\mu n + \varsigma - 2t\gamma}{2\sqrt{t}} \right] + \mathrm{erf}\left[\frac{\mu - 2\mu n - \varsigma + 2t\gamma}{2\sqrt{t}} \right] \right.$$
$$\left. + \mathrm{e}^{2\gamma(2\mu n + \varsigma)} \left(\mathrm{erf}\left[\frac{\mu + 2\mu n + \varsigma + 2t\gamma}{2\sqrt{t}} \right] - \mathrm{erf}\left[\frac{2\mu n + \varsigma + 2t\gamma}{2\sqrt{t}} \right] \right) \right) H(t) \tag{40}$$

where erf[z] is the error function:

$$\mathrm{erf}[z] = \frac{2}{\sqrt{\pi}} \int_0^z \mathrm{e}^{-\xi^2} \mathrm{d}\xi$$

Another limit case is the pure wave equation. A solution in this case can be written as:

$$\vartheta = \mathrm{e}^{-\varsigma\gamma} H(t) - 2\mu\gamma \mathrm{e}^{-\mu\gamma} \sum_{n=1}^{\infty} \frac{\cos\left[\frac{n\pi\varsigma}{\mu}\right] \left(1 - \cos\left[\frac{n\pi t}{\mu\sqrt{\tau}}\right]\right) (\mathrm{e}^{\mu\gamma} - (-1)^n)}{n^2\pi^2 + \mu^2\gamma^2} H(t) \tag{41}$$

An expression for the temperature (39) on the wave front as a function of coordinate ς can be obtained as a special case ($t = \varsigma\sqrt{\tau}$) of the solution for an abrupt heat source given in work [21] for a half-space. The temperature value ϑ_1 at the wave front if the wave has not reached the right boundary is given as follows:

$$\vartheta_1(\varsigma) = \frac{1}{2r} \left((r+1)\mathrm{e}^{\frac{r\varsigma}{\sqrt{\tau}}} + r - 1 \right) \mathrm{e}^{-\frac{(r+1)\varsigma}{2\sqrt{\tau}} - \gamma\varsigma}; \quad r = \sqrt{4\gamma^2\tau + 1} \tag{42}$$

Time profiles of the solutions (39)–(41) are shown in Fig. 4 with the same scale of the horizontal axis, but with different scales of the vertical axis. The solution of the hyperbolic heat Eq. (39) is shown in Fig. 4a and b. The temperature values on the wave front (42) are shown by dashed lines in Fig. 4a and b. The solution (41) of the wave equation is shown in Fig. 4c, and the solution (40) of the classic heat equation is shown in Fig. 4d.

A temperature maximum is observed at small times in the salient point near the exposed boundary of the layer (Fig. 4a). This effect is noticeable in hyperbolic heat conduction problems with various dependencies of internal heat sources on time [21]. Such maximum is also observed in the solution of the wave equation (Fig. 4c) for all values of t. Time profiles in Fig. 4a with increasing time (the curves $t = 8\tau$) become similar to the monotonically decreasing classic solution in Fig. 4d: the temperature maximum is shifting from the inner part of the layer to its boundary.

The problem (29)–(30) is a generalization of the boundary-value problem (15)–(16) for the case of the volumetric impact. In the solution graphics of the boundary-value problem (19), a discontinuous jump can be observed instead of the salient point. The graphic vanishes right after the wave front as it is shown in Fig. 1a and b. The solution graphs of the problem with the volumetric heat source (Fig. 4a) gradually decay after attaining a maximum at its wave front. At the same time, the solution profiles for the classic thermoconductivity of both problems shown in Figs. 4d and 1d are quite similar in shape.

The solution profiles of (39) are shown in Fig. 5 for various γ values ($\gamma_1 < \gamma_2 < \gamma_3$) but at the same moment of time. The γ constant characterizes a penetration depth of the laser radiation into the medium. With the increase in γ, the temperature at the border decreases and the temperature maximum becomes more noticeable. With decreasing of γ, the curves become similar to the classical solution (Fig. 4d).

Let us consider the reflection of the heat wave from the opposite boundary of the layer. We assume that the layer is thin enough so the wave does not completely decay until it reaches the opposite border. In Fig. 6a,

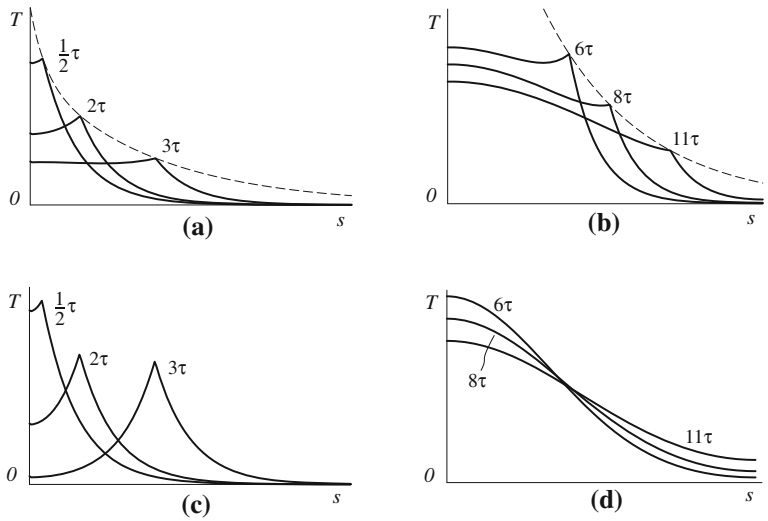

Fig. 4 Volumetric heat supply is considered. Boundaries of the layer are thermally insulated. Solution profiles for the different time values are presented: $\tau/2$, 2τ, 5τ, 6τ, 8τ, 11τ seconds; curves **a**, **b** are the solution profiles corresponding to the hyperbolic heat equation; curve **c** is the solution profile corresponding to the wave equation; curve **d** is the solution profiles corresponding to the classic parabolic heat equation

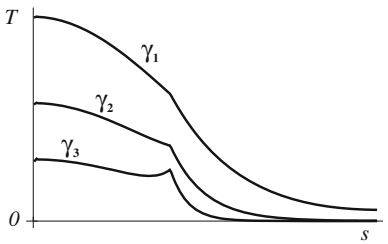

Fig. 5 Solution profiles for the hyperbolic heat equation at the same moment of time, but for different values of attenuation coefficient: $\gamma_1 < \gamma_2 < \gamma_3$

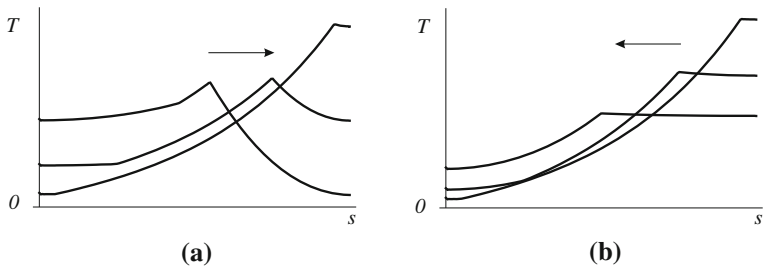

Fig. 6 Reflection of the heat wave from the opposite boundary under the conditions of thermal insulations of the layer

the wave is moving from left to right and in Fig. 6b from right to left. Upon reflection from the boundary, the temperature reaches its local maximum [22], which gradually approaches to a constant value with time.

Let us consider the behavior of the temperature at the boundary of the layer, where it is the easiest to measure. The temperature dependence on time at the exposed boundary is shown in Fig. 7a and the dependence $T(t)$ at the opposite boundary is shown in Fig. 7b. The presence of maximums and minimums on the graph of the hyperbolic solution (which is shown by the solid line) is the result of the heat wave movement in the layer (Fig. 6). The graph of the classic solution is monotonous (dashed line) and decays faster. The value of $T(t)$ approaches a constant value with increasing time both in classic and hyperbolic heat conduction theories.

Taking into account the wave nature of heat propagation, it is necessary to make substantial changes in the thermal insulation methods. The effect of the total internal reflection at the interface of two media has been known from optics and acoustics [23]. The boundary of the medium will be an absolute reflector of heat

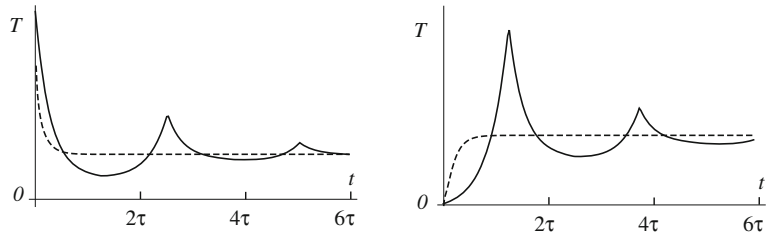

Fig. 7 The temperature dependence on time at the boundary of a thin layer. **a** Temperature at the irradiated boundary; **b** temperature at the opposite boundary

waves if a wave strikes it at an angle larger than a critical angle Θ. If the wave propagation speed in the second medium is greater than in the first medium ($c_1 < c_2$), then the critical angle Θ is given by $\sin\Theta = c_1/c_2$. In the notations of the hyperbolic thermal conductivity theory, the heat propagation velocity can be rewritten as $c = \sqrt{\lambda/(\rho C_v \tau)}$.

4.1.2 The boundaries of the layer are kept at the constant temperature

Differential equation for the temperature (7) in the notation (28) takes the form:

$$\dot{\vartheta} + \tau\ddot{\vartheta} - \vartheta'' = (\delta(t-0) + \tau\dot{\delta}(t-0))\mathrm{e}^{-\gamma\varsigma} \tag{43}$$

Initial conditions (8) for the temperature are as follows:

$$\vartheta\big|_{t=0} = 0; \quad \dot{\vartheta}\big|_{t=0} = 0; \tag{44}$$

The boundary conditions are:

$$\vartheta\big|_{\varsigma=0} = 0; \quad \vartheta\big|_{\varsigma=\mu} = 0; \tag{45}$$

Let us make the variable change in Eq. (43):

$$\vartheta(\varsigma, t) = \exp\left(-\frac{t}{2\tau}\right) w(\varsigma, t) \tag{46}$$

After the variable changes, Eq. (43) will be as follows:

$$\ddot{w} = \frac{1}{\tau}w'' + \frac{1}{4\tau^2}w + \left(\frac{\delta(t-0)}{2\tau} + \dot{\delta}(t-0)\right)\mathrm{e}^{-\gamma\varsigma} \tag{47}$$

The initial and boundary conditions will take a form:

$$w\big|_{t=0} = 0; \quad \dot{w}\big|_{t=0} = 0; \quad w\big|_{\varsigma=0} = 0; \quad w\big|_{\varsigma=\mu} = 0; \tag{48}$$

To obtain a solution of the problem (47), (48), we use formula (37). Substituting $w(\varsigma, t)$ into (46), we obtain an expression for the temperature $\vartheta(\varsigma, t)$:

$$\begin{aligned}\vartheta = 2\pi\mathrm{e}^{-\mu\gamma-\frac{t}{2\tau}} \sum_{n=1}^{\infty} \frac{n\left(\mathrm{e}^{\mu\gamma} - (-1)^n\right)\sin\left[\frac{n\pi\varsigma}{\mu}\right]}{S_n\left(n^2\pi^2 + \mu^2\gamma^2\right)} \\ \times\left(S_n\cos\left[\frac{1}{2}S_n t\right] + \mu\sin\left[\frac{1}{2}S_n t\right]\right) H(t)\end{aligned} \tag{49}$$

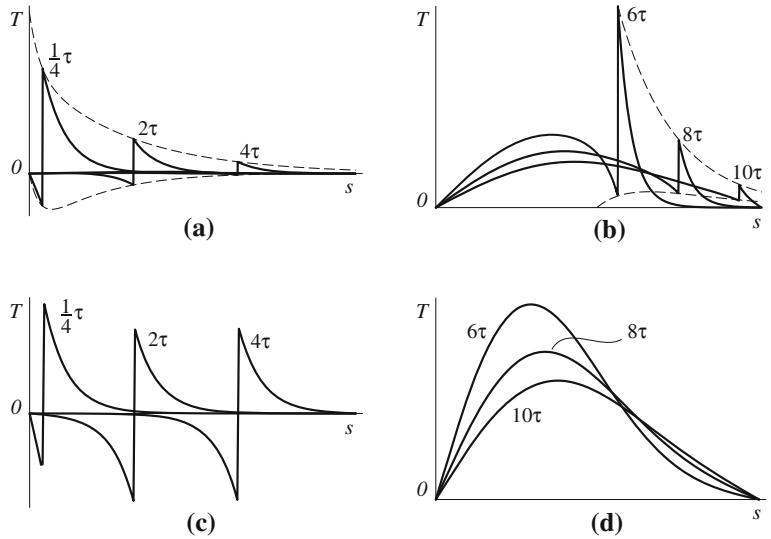

Fig. 8 Volumetric heat supply is considered. Boundaries of the layer are kept at a constant temperature. Solution profiles for the different time values are presented: $\tau/4$, 2τ, 4τ, 6τ, 8τ, 10τ seconds; curves **a**, **b** are the solution profiles corresponding to the hyperbolic heat equation; curve **c** is the solution profile corresponding to the wave equation; curve **d** is the solution profile corresponding to the classic parabolic heat equation

The convergence of this series is considered in the "Appendix." A solution for the layer with the constant temperature at the boundaries in the classic thermal conductivity is given as follows:

$$\vartheta = \frac{e^{\gamma(t\gamma-\varsigma)}}{2}\sum_{n=-\infty}^{\infty} e^{-2\mu n\gamma}\left(\operatorname{erf}\left[\frac{2\mu n+\varsigma-2t\gamma}{2\sqrt{t}}\right]+\operatorname{erf}\left[\frac{\mu-2\mu n-\varsigma+2t\gamma}{2\sqrt{t}}\right]\right.$$
$$\left.+\, e^{2(2\mu n+\varsigma)\gamma}\left(\operatorname{erf}\left[\frac{2\mu n+\varsigma+2t\gamma}{2\sqrt{t}}\right]-\operatorname{erf}\left[\frac{\mu+2\mu n+\varsigma+2t\gamma}{2\sqrt{t}}\right]\right)\right)H(t) \tag{50}$$

Using the method of Green's functions, we obtain a solution for the wave equation:

$$\vartheta = 2\pi e^{-\mu\gamma}\sum_{n=1}^{\infty}\frac{n\cos\left[\frac{n\pi t}{\mu\sqrt{\tau}}\right](e^{\mu\gamma}-(-1)^n)\sin\left[\frac{n\pi\varsigma}{\mu}\right]}{n^2\pi^2+\mu^2\gamma^2}H(t) \tag{51}$$

The values of temperature on the wave front are different because of the discontinuity jump. The temperature value at the wave front approaching from right is given by (42). The temperature value at the wave front approaching from left is given by:

$$\vartheta_2(\varsigma) = \vartheta_1(\varsigma) - e^{-\frac{\varsigma}{2\sqrt{\tau}}} \tag{52}$$

The solution of the hyperbolic heat Eq. (49) is shown in Fig. 8a and b. The temperature values on the wave front are shown by dashed lines in Fig. 8a and b. The upper dashed line is given by (42) and the lower dashed line is given by (52). The solution of the wave equation is shown in Fig. 8c, and the solution of the classic heat Eq. (50) is shown in Fig. 8d. Pairs of the figures: Fig. 8a, c and b, d has the same scale of the horizontal axes, but different scales of the vertical axes.

Under the considered boundary conditions, one can observe areas where the temperature drops below its initial value, such areas have negative values of T. Global maximum and minimum values of the temperature are reached in a thin layer near the irradiated boundary. For short times (curves $t = \tau/2$), the solution profile of the hyperbolic equation (Fig. 8a) is similar to the solution profile of the wave equation (Fig. 8c): a temperature minimum that lies in the region of the negative T and a significant gap between the minimum and the maximum by the T axis can be observed. Over time the minimum and maximum approach each other (Fig. 8b), the minimum of the solution curve leaves the range of negative values and the graph becomes similar to the classic one (Fig. 8d).

Let us consider in detail the area with negative values of T in solution (49). We shall assume that the temperature wave has not reached the right boundary of the layer, so the layer can be treated as a half-space. Taking the Laplace transform of Eq. (43) using the initial conditions (44), one obtains:

$$p\overline{\vartheta} + \tau p^2\overline{\vartheta} - \overline{\vartheta}'' = (1 + \tau p)\mathrm{e}^{-\gamma\varsigma} \tag{53}$$

where

$$\overline{\vartheta}(\varsigma, p) = L[\vartheta(\varsigma, t)] \tag{54}$$

The transformed boundary conditions are given by:

$$\overline{\vartheta}\big|_{\varsigma=0} = 0; \quad \overline{\vartheta}\big|_{\varsigma\to\infty} = 0; \tag{55}$$

A solution for the problem (53), (55) is the following function:

$$\overline{\vartheta}(\varsigma, p) = \frac{(p\tau + 1)\mathrm{e}^{-\varsigma\left(\gamma+\sqrt{p(p\tau+1)}\right)}\left(\mathrm{e}^{\varsigma\sqrt{p(p\tau+1)}} - \mathrm{e}^{\gamma\varsigma}\right)}{p^2\tau + p - \gamma^2} \tag{56}$$

The Taylor expansion of (56) at infinity by variable p and at 0 by variable ς is given as follows:

$$\overline{\vartheta}(\varsigma, p) = \frac{\varsigma\left(2p\tau - 2\gamma\sqrt{\tau} + 1\right)}{2p\sqrt{\tau}} + O(\varsigma)^2 + O\left(\frac{1}{p}\right)^{3/2} \tag{57}$$

Taking the inverse Laplace transform of (57), one obtains [24] the first term of Taylor series for $\vartheta(\varsigma, t)$ at $(0, 0)$:

$$\vartheta(\varsigma, t) \approx \left(\frac{x}{2\sqrt{\tau}} - \gamma x\right) H(t) + \sqrt{\tau} x\delta(t) \tag{58}$$

For $t > 0$, it is possible to evaluate when the temperature ϑ takes positive or negative values in the vicinity of the irradiated boundary. It depends on a relationship between the heat flux relaxation constant τ in a medium and a value of τ_0:

$$\tau_0 = \frac{1}{4\gamma^2} \tag{59}$$

If $\tau > \tau_0$, then ϑ takes negative values in the vicinity of the irradiated boundary; otherwise, if $\tau < \tau_0$, ϑ takes positive values.

Let us estimate the constant τ_0 for typical metals (e.g., aluminum, copper, gold, and silver). As it was stated above (28): $\gamma = \alpha\sqrt{\lambda/(\rho C_v)}$. The value of the square root for the considered metals is approximately $\sqrt{\lambda/(\rho C_v)} \approx 0.01$. The value of the absorbtion coefficient can be estimated as $\alpha = \varepsilon^{-1}$, where the ε is a skin depth [25]. The skin depth significantly depends on frequency (or signal duration): within the range from 10 GHz to 1 THz, it varies from 10^{-6} to 10^{-7} m [25]. The continuum mechanics approach is still valid for such frequencies [26]. Consequently, the value of τ_0 varies from 10^{-9} to 10^{-11} s. These values match the estimations of τ for metals and solids [7] by the order of magnitude.

Temperature profiles (49) for the case of $\tau < \tau_0$ are plotted in Fig. 9. The effect of cooling near the irradiated boundary is not observed.

Function $\dot{\delta}(t)$ can be rewritten as $\delta(t)/t$, so it can be easily seen that $\dot{\delta}(t)$ has negative values if approaching from the left and positive values if approaching from the right. The negative values at the right-hand sight of a nonhomogeneous wave equation lead to negative peaks in solution (51) plotted in Fig. 8c. Generally, if the impulse decays within some period of time, then the derivative $\tau\dot{q}$ (7) will also have negative values. These negative values will be the more noticeable the faster q decays with time and the greater τ constant is.

Curves in Fig. 10 pass through the minimums of $T(s)$, which are found at different moments of time. Coordinate s is plotted along the horizontal axis. It is assumed that the opposite boundary of the layer is sufficiently far from the irradiated boundary and does not affect the results. In Fig. 10, three curves are built for the different values of the heat flux relaxation constant: $\tau_1 < \tau_2 < \tau_3$. Each curve comes out of the coordinate origin, has the only minimum ($|\theta_1| < |\theta_2| < |\theta_3|$), and reaches the horizontal axis over the certain time

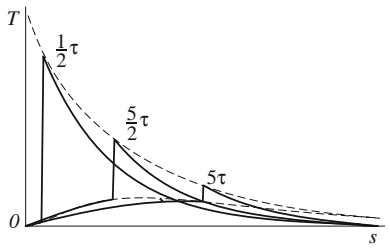

Fig. 9 Volumetric heat supply is considered. Boundaries of the layer are kept at a constant temperature. Solution profiles corresponding to the hyperbolic heat equation for the different time values are presented: $\tau/2$, $5\tau/2$, 5τ seconds. Cooling areas in the vicinity of the irradiated boundary are not observed

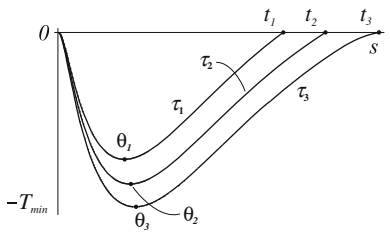

Fig. 10 Temperature minima near the boundary of the layer, exposed to the short laser impulse

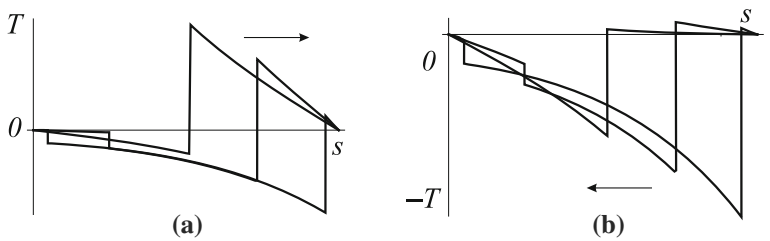

Fig. 11 Reflection of the heat wave from the opposite boundary. The temperature at the boundaries is kept constant

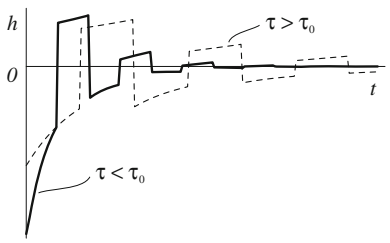

Fig. 12 Dependence of the heat flux at the irradiated boundary on time

interval: $t_1 < t_2 < t_3$. Numerical analysis shows that with the increasing of the heat flux relaxation constant, the absolute temperature minimum $\theta = \min T(s, t)$ is shifted deeper into the layer.

In Fig. 11a, the wave is moving from left to right and in Fig. 11b from right to left. The amplitude of the temperature wave changes its sign when reflecting from the opposite boundary, which is typical for the wave equation under the considered boundary conditions.

Let us consider heat flux η at the irradiated boundary of the layer. Introducing temperature (49) into expression (14) for a heat flux and assuming $\varsigma = 0$, one obtains:

$$\eta(t) = 4\pi^2 \mathrm{e}^{-\gamma\mu - \frac{t}{2\tau}} \sum_{n=1}^{\infty} \frac{\left((-1)^n - \mathrm{e}^{\gamma\mu}\right) n^2 \sin\left(\frac{t S_n}{2\mu\tau}\right)}{\left(\gamma^2\mu^2 + \pi^2 n^2\right) S_n} \tag{60}$$

Curves in Fig. 12 were plotted for the heat flux at the irradiated boundary (60) upon the following conditions: $\tau > \tau_0$ for the dashed curve and $\tau < \tau_0$ for the solid curve. The value of the heat flux (60) at the initial moment

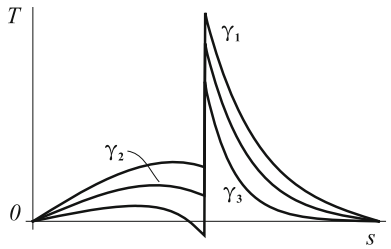

Fig. 13 Solution profiles for the hyperbolic heat equation at the same moment of time, but for different values of attenuation coefficient: $\gamma_1 < \gamma_2 < \gamma_3$

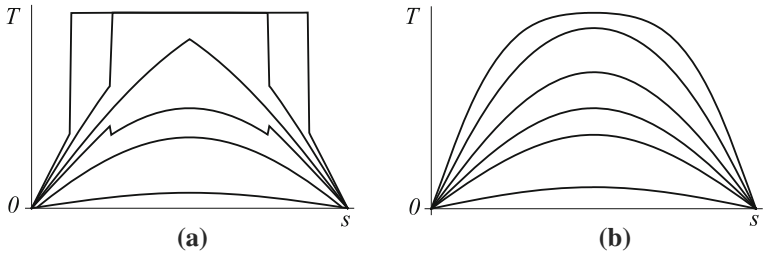

Fig. 14 The temperature distributions in the uniformly ($\gamma = 0$) heated layer gradually cooling under the boundary conditions of the first kind

of time is a finite quantity and it increases along with decreasing heat flux relaxation constant. If τ tends to zero (the classic thermoconductivity limit case), then the value of the heat flux at $t = 0$ tends to infinity. The effect of cooling at the vicinity of the irradiated boundary is observed at the lower absolute values of the heat flux (dashed curve in Fig. 12).

If the temperature wave with positive peak values reaches the boundary (Fig. 11), then the heat flux changes its sign to negative (or in other words turns outwards the layer) undergoing a discontinuity jump (Fig. 12). If a "negative wave" reaches the boundary, then the heat flux becomes positive (turns inwards the layer). Due to unrestricted value of the heat flux at the boundaries, it is possible to emit or absorb any amount of energy needed to invert the sign of wave peak values. In the case of thermal insulation, wave peak values do not change their signs reflecting from the boundaries (Fig. 6). If some conditions are imposed on the heat flux, then peak values will be inverted just partly.

The effect of the temperature lowering below its initial value is observed under the considered boundary conditions with unrestricted heat flux at the boundaries. In papers [27,28], it is stated that free heat exchange is difficult to reproduce due to a high thermal resistance at the interface between nanoscale objects.

The temperature lowering below its initial value is the intrinsic part of hyperbolic model (7). To obtain correct results in the vicinity of the absolute zero, it is necessary to use the Debye model [29], which incorporates the nonlinear temperature dependence on the heat capacity, which is proportional to T^3.

Since the present resolution of testing devices (10^{-3} m by the coordinate [16]) is not sufficient to observe hyperbolic heat conduction effects directly because it is recognized that such effects decay at a distance of few nanometers [4], existing experimental data cannot prove or disprove theoretically predicted effects. Many contradictory experimental results can be found in the literature: [30–35]. With further development of technology, it would be possible to clarify the matter.

Increasing of constant γ lowers the values of maximums and minimums in the temperature graphs. The lower curve in Fig. 13 corresponds to the larger value of constant γ ($\gamma_1 < \gamma_2 < \gamma_3$). The larger the γ is, the more noticeable the negative minimum of T becomes and the longer time they can be observed. Decreasing of γ does not make the curves more similar to the classic solution (Fig. 8d) unlike the previously considered problem.

Let us consider the special case of the solution (49) if $\gamma = 0$. It is possible if the laser power does not decrease with the distance from the border and heat is supplied into the volume uniformly throughout its thickness. A thin, evenly heated from aside along its length rod can be an example. Since its boundaries are kept under a constant temperature, it gradually cools down. Time profiles for the special case of the solution (49) are shown in Fig. 14a for the different moments of time (top to bottom): $t = \tau, 2\tau, 4\tau, 6\tau, 8\tau$, and 16τ. Profiles of the classic solution for the same moments of time are represented in Fig. 14b. The salient points

and discontinuities can be observed on the first few curves, but with time the curves merge with the classic solution. The temperature propagation process in this case can be observed by, for example, a thermovision camera, if it possesses the appropriate resolution by coordinate and time.

If the characteristic times of the heat transfer process are sufficiently small so that it can be considered as a wave process, then one can use a quarter-wave antireflection coating [23] to minimize the waves reflection from the interface between two media. Parameters of such coating film should satisfy the well-known ratio: $Z_{1/4} = \sqrt{Z_1 Z_2}$, where Z_1 and Z_2 are wave resistances of the media on the left and on the right side of the antireflection coating film. In the notation of the hyperbolic heat conduction theory, $Z = \sqrt{\lambda \rho C_v / \tau}$.

4.2 The intensity of the internal heat sources depends on time as the Heaviside step function

Let us consider the continuous exposure of the layer to the laser radiation. The intensity of the internal heat sources $q(s, t)$ is constant in time:

$$q = I_0 H(t-0) \mathrm{e}^{-\alpha s} \tag{61}$$

4.2.1 The thermally insulated layer

Differential equation for the heat flux (11) with regard to (61) can be written as follows:

$$\dot{\eta} + \tau \ddot{\eta} - \eta'' = \gamma H(t-0) \mathrm{e}^{-\gamma \varsigma} \tag{62}$$

The notations, boundary, and initial conditions are the same as in the problem (29)–(31). Following the procedure used above, we obtain an expression for the temperature:

$$\vartheta = \mathrm{e}^{-\varsigma\gamma} t H(t) - 2\mu\gamma \mathrm{e}^{-\mu\gamma} \sum_{n=1}^{\infty} \left(\frac{((-1)^n - \mathrm{e}^{\mu\gamma}) \cos\left[\frac{n\pi\varsigma}{\mu}\right]}{n^2\pi^2 \left(n^2\pi^2 + \mu^2\gamma^2\right)} \left(\mu^2 - n^2\pi^2 t \right.\right.$$
$$\left.\left. - \mathrm{e}^{-\frac{t}{2\tau}} \mu \left(\mu \cos\left[\frac{t S_n}{2\tau\mu}\right] + \frac{\mu^2 - 2n^2\pi^2\tau}{S_n} \sin\left[\frac{t S_n}{2\tau\mu}\right] \right) \right) \right) H(t) \tag{63}$$

A solution of this problem in the classic formulation is:

$$\vartheta = \frac{\left(1 - \mathrm{e}^{-\mu\gamma}\right) t}{\mu\gamma} H(t)$$
$$+ 2\mu^3\gamma \sum_{n=1}^{\infty} \frac{(\mathrm{e}^{\mu\gamma} - (-1)^n) \cos\left[\frac{n\pi\varsigma}{\mu}\right] \mathrm{e}^{-\mu\gamma} \left(1 - \exp\left(-\frac{n^2\pi^2 t}{\mu^2}\right)\right)}{n^2\pi^2 \left(n^2\pi^2 + \mu^2\gamma^2\right)} H(t) \tag{64}$$

In the limit case of the wave equation, an expression for ϑ is written as follows:

$$\vartheta = \mathrm{e}^{-\varsigma\gamma} t H(t) - 2\mu\gamma \mathrm{e}^{-\mu\gamma}$$
$$\times \sum_{n=1}^{\infty} \frac{((-1)^n - \mathrm{e}^{\mu\gamma}) \cos\left[\frac{n\pi\varsigma}{\mu}\right] \left(\mu\sqrt{\tau} \sin\left[\frac{n\pi t}{\mu\sqrt{\tau}}\right] - n\pi t\right)}{n\pi \left(n^2\pi^2 + \mu^2\gamma^2\right)} H(t) \tag{65}$$

The temperature value on the wave front ($t = \varsigma\sqrt{\tau}$) can be obtained as a special case of the solution [21] for the half-space:

$$\vartheta_3(\varsigma) = \frac{1}{2\gamma^2 r} \mathrm{e}^{-\frac{(r+1)x}{2\sqrt{\tau}} - \gamma x} \left(\left(2\gamma^2\tau + r + 1\right) \mathrm{e}^{\frac{rx}{\sqrt{\tau}}} - 2\gamma^2\tau - 2r\mathrm{e}^{\frac{(r+1)x}{2\sqrt{\tau}}} + r - 1 \right) \tag{66}$$

The solution graphics of the hyperbolic heat conduction equation (Fig. 15) monotonously decrease at all values of time: they have no salient points or jumps, typical for the previously concerned problems. The dashed line given by (66) intersects the temperature profiles at the points of inflexion (Fig. 16).

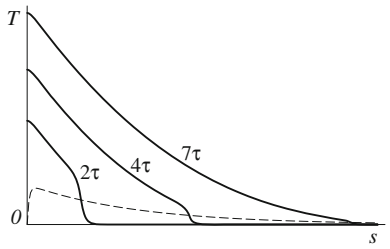

Fig. 15 Volumetric heat supply is considered. Boundaries of the layer are thermally insulated. Solution profiles corresponding to the hyperbolic heat equation for the different time values are presented

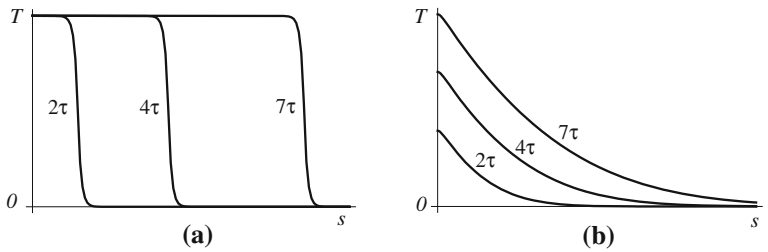

Fig. 16 Volumetric heat supply is considered. Boundaries of the layer are thermally insulated. Solution profiles corresponding to the wave equation (**a**) and to the classic parabolic heat equation (**b**) for the different time values are presented

If the attenuation of the laser radiation in the layer is significant, then the solution profiles in Fig. 15 are similar to the solution profiles in Fig. 16a at short times ($t = 2\tau$). Curves in Fig. 15 become similar to the curves for the classic heat conduction problem (Fig. 16b) with increasing of time ($t = 8\tau$) or with decreasing of the attenuation coefficient γ in the medium. Furthermore, the solution becomes similar to the solution of the boundary-value problem (Fig. 2b) with increasing of the attenuation coefficient: T values quicker reach zero after its "wave front." Classic solution curves (Figs. 2, 16b) are similar.

4.2.2 The boundaries are kept at a constant temperature

Differential equation for the temperature (7) with heat source (61) is written as follows:

$$\dot{\vartheta} + \tau\ddot{\vartheta} - \vartheta'' = (H(t-0) + \tau\delta(t-0))\mathrm{e}^{-\gamma\varsigma} \tag{67}$$

The notations, boundary, and initial conditions are the same as in the problem (43)–(45). Following the procedure used above, we obtain an expression for the temperature:

$$\vartheta = 2\mu^2\mathrm{e}^{-\mu\gamma}\sum_{n=1}^{\infty}\frac{(\mathrm{e}^{\mu\gamma}-(-1)^n)\sin\left[\frac{n\pi\varsigma}{\mu}\right]}{n\pi\left(n^2\pi^2+\mu^2\gamma^2\right)} \times\left(1-\mathrm{e}^{-\frac{t}{2\tau}}\left(\frac{\mu^2-2n^2\pi^2\tau}{\mu S_n}\sin\left[\frac{tS_n}{2\tau\mu}\right]+\cos\left[\frac{tS_n}{2\tau\mu}\right]\right)\right)H(t) \tag{68}$$

A solution of the problem in the classic formulation can be written as follows:

$$\vartheta = \sum_{n=1}^{\infty}\frac{2\left(-(-1)^n+\mathrm{e}^{\mu\gamma}\right)\mu^2+\mathrm{e}^{-\mu\gamma}\left(1-\exp\left(-\frac{n^2\pi^2t}{\mu^2}\right)\right)\sin\left[\frac{n\pi\varsigma}{\mu}\right]}{n\pi\left(n^2\pi^2+\mu^2\gamma^2\right)}H(t) \tag{69}$$

In the limit case of the wave equation, an expression for ϑ is written as follows:

$$\vartheta = 2\mu\sqrt{\tau}\mathrm{e}^{-\mu\gamma}\sum_{n=1}^{\infty}\frac{(-(-1)^n+\mathrm{e}^{\mu\gamma})\sin\left[\frac{n\pi\varsigma}{\mu}\right]\sin\left[\frac{n\pi t}{\mu\sqrt{\tau}}\right]}{n^2\pi^2+\mu^2\gamma^2}H(t) \tag{70}$$

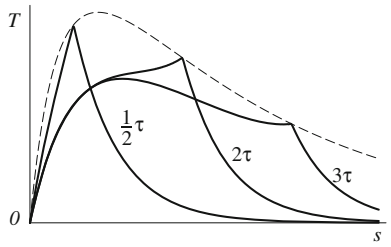

Fig. 17 Volumetric heat supply is considered. Boundaries of the layer are kept at a constant temperature. Solution profiles corresponding to the hyperbolic heat equation for the different time values are presented

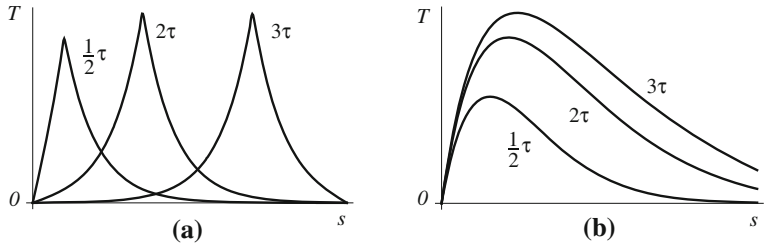

Fig. 18 Volumetric heat supply is considered. Boundaries of the layer are kept at a constant temperature. Solution profiles corresponding to the wave equation (**a**) and to the classic parabolic heat equation (**b**) for the different time values are presented

Unlike the temperature graphics for the layer under the influence of the short laser impulse (Fig. 4a), the graphics in Fig. 17 do not have the region of negative temperatures in the vicinity of the irradiated surface of the layer. The temperature values on the wave front (66) are shown by the dashed line in Fig. 17.

For short times (curves $t = \tau/2$), the solution profile of the hyperbolic equation (Fig. 17) is similar to the solution profile of the wave equation (Fig. 18a): the temperature reaches its maximum at the salient point and then quickly decays. With increasing of time (curves $t = 3\tau$), a second extremum point which is similar to the extremum point of the classic curves (Fig. 18b) appears and the salient point ceases to be a global maximum.

5 Conclusion

In this work, we obtained and investigated the solutions of various hyperbolic heat conduction problems for a layer under the influence of laser pulses. It is shown in several examples that in a short time of the order of the heat flux relaxation constant $t \sim \tau$ and at distances from the irradiated surface of the order of $s \sim c\tau$ (where $c = \sqrt{\lambda/(\rho C_v \tau)}$ is the heat propagation speed in the medium), the solution of the hyperbolic heat equation is similar to the solution of the wave equation. If times are one order of magnitude greater than τ, the hyperbolic solution is practically indistinguishable from the classic solution.

The temperature values at the boundaries and the temperature distribution inside the uniformly heated layer were plotted for the convenient comparison of the results with experimental data.

Two types of heat conduction problems that simulate the exposure of the layer to laser radiation where considered: laser radiation heats only the surface of the material (the heat flux is specified at the boundary) and the laser radiation penetrates into a skin layer, the thickness of which is characterized by the attenuation coefficient α (the distribution of the heat sources is specified in the material volume).

If the heat flux applied at the boundary depends on time as the δ function, then the discontinuity jump will be observed at the thermal wave front. In the layer with the distributed heat sources, the power of which depends on time as the δ function, salient points can be observed instead of the discontinuity jump at the front.

The problems, which concern the heat flux, and the power of internal heat sources, which depend on time as the Heaviside step function, are also investigated. It is shown that in the boundary-value problem, the temperature graph breaks at the wave front, while the solution graphics for the problem concerning the volumetric sources decrease to zero gradually.

Under homogeneous boundary conditions, one can observe the areas where the temperature drops below its initial value (Figs. 8a, b, d, 17d) or the areas where the solution graph has two extreme points. The solution graphs of the hyperbolic heat conduction problem with homogeneous boundary conditions differ

more significantly from the classic limit case and retain their differences for longer than under the boundary conditions of thermal insulation.

If $\tau > \tau_0$ (59), the temperature in the vicinity of the irradiated boundary drops below its initial value for a short time to the order of the τ constant in the medium. The lifetime of the negative temperature minimum increases along with the heat flux relaxation constant. The greater the τ constant, the lower the absolute temperature minimum $\theta = \min T(s, t)$ is. The numerical analysis shows that for a fixed τ, it is possible to find an optimal value for the laser attenuation constant γ_* and the value of θ will be minimal.

Experimental determination of the heat flux relaxation constant τ presents a challenging problem. A number of authors [30–35] give conflicting results that differ by orders of magnitude. The paper [35] gives an overview of publications devoted to the experimental determination of the constant τ and a comparative table of the empirically obtained values of τ from the papers [31–34]. The values of τ given in these papers range from a few seconds to tens of seconds. On the other hand, there is a theoretical estimation of the heat flux relaxation time based on the phonon theory [36]. According to this estimation, the values of τ are ten orders of magnitude smaller than it is stated in the above publications. For example, $\tau_{Al} \approx 10^{-11}$ s for aluminum. By the period of time $t = \tau_{Al}$, the heat wave will travel the distance $s \approx 3 \times 10^{-8}$ m which is five orders of magnitude less than the available coordinate resolution (10^{-3} m) of the existing temperature measurement methods [16]. However, if the value of τ is close to the values presented in the works [31–34], then nonclassical effects presented in this article should be observed at larger scales.

Acknowledgments The authors are deeply grateful to D.A. Indeitsev, D.P. Kouzov, and A.M. Krivtsov for helpful discussions.

Appendix

Let us decompose (49) into the sum of series. Here, we consider the convergence proof of one of them (the convergence of other series can be easily proved):

$$\sum_{n=1}^{\infty} \frac{n \cos\left[\frac{t\sqrt{4n^2\pi^2\tau-\mu^2}}{2\mu\tau}\right] \sin\left[\frac{n\pi\varsigma}{\mu}\right]}{n^2\pi^2 + \mu^2\gamma^2} \tag{71}$$

(ς, t are the coordinate and time: μ, τ, γ are positive constants)
According to the Dirichlet's convergence test, whether the sequence of partial sums is limited:

$$\left| \sum_{k=1}^{n} \cos\left[\frac{t\sqrt{4k^2\pi^2\tau - \mu^2}}{2\mu\tau}\right] \sin\left[\frac{k\pi\varsigma}{\mu}\right] \right| \le M$$

and the series:

$$\sum_{n=1}^{\infty} \frac{n}{n^2\pi^2 + \mu^2\gamma^2}$$

monotonically approaches zero beginning from some number n, then the series (71) converges.

Proof If $n < \infty$, then one can always find such a positive M that

$$\left| \sum_{k=1}^{n} \cos\left[\frac{t\sqrt{4k^2\pi^2\tau - \mu^2}}{2\mu\tau}\right] \sin\left[\frac{k\pi\varsigma}{\mu}\right] \right| \le M \tag{72}$$

If $n \to \infty$, then the expression under the cos can be expended into the asymptotic series for large k:

$$\frac{t\sqrt{4k^2\pi^2\tau - \mu^2}}{2\mu\tau} = \frac{\pi t k}{\mu\sqrt{\tau}} + O\left[\frac{1}{k^1}\right]$$

Let us rewrite the cos from (72) in the following form:

$$\cos\left[\frac{t\sqrt{4k^2\pi^2\tau-\mu^2}}{2\mu\tau}\right]=\left(\cos\left[\frac{t\sqrt{4k^2\pi^2\tau-\mu^2}}{2\mu\tau}\right]-\cos\left[\frac{\pi tk}{\mu\sqrt{\tau}}\right]\right)+\cos\left[\frac{\pi tk}{\mu\sqrt{\tau}}\right]$$
$$=-2\sin\left[\frac{t\sqrt{4k^2\pi^2\tau-\mu^2}}{4\tau\mu}-\frac{\pi tk}{2\mu\sqrt{\tau}}\right]\sin\left[\frac{\pi tk}{2\mu\sqrt{\tau}}+\frac{t\sqrt{4k^2\pi^2\tau-\mu^2}}{4\tau\mu}\right]+\cos\left[\frac{\pi tk}{\mu\sqrt{\tau}}\right]$$

Let us make an estimation:

$$\cos\left[\frac{t\sqrt{4k^2\pi^2\tau-\mu^2}}{2\mu\tau}\right]\le 2\left|\sin\left[\frac{t\sqrt{4k^2\pi^2\tau-\mu^2}}{4\tau\mu}-\frac{\pi tk}{2\mu\sqrt{\tau}}\right]\right|\times 1+\left|\cos\left[\frac{\pi tk}{\mu\sqrt{\tau}}\right]\right|$$

If $k\to\infty$

$$\left|\sin\left[\frac{t\sqrt{4k^2\pi^2\tau-\mu^2}}{4\tau\mu}-\frac{\pi tk}{2\sqrt{\tau}\mu}\right]\right|=\left|O\left[\frac{1}{k^1}\right]\right|$$

then

$$2\left|\sin\left[\frac{t\sqrt{4k^2\pi^2\tau-\mu^2}}{4\tau\mu}-\frac{\pi tk}{2\sqrt{\tau}\mu}\right]\right|+\left|\cos\left[\frac{\pi tk}{\mu\sqrt{\tau}}\right]\right|=2\left|O\left[\frac{1}{k^1}\right]\right|+\left|\cos\left[\frac{\pi tk}{\mu\sqrt{\tau}}\right]\right|$$

Substituting obtained estimation into the expression (72), we obtain:

$$\left|\sum_{k=1}^{n}\cos\left[\frac{t\sqrt{4k^2\pi^2\tau-\mu^2}}{2\mu\tau}\right]\sin\left[\frac{k\pi\varsigma}{\mu}\right]\right|$$
$$\le\left|\sum_{k=1}^{n}\left(2\left|O\left[\frac{1}{k^1}\right]\right|+\left|\cos\left[\frac{\pi tk}{\mu\sqrt{\tau}}\right]\right|\right)\sin\left[\frac{k\pi\varsigma}{\mu}\right]\right|$$
$$=\left|\sum_{k=1}^{n}\left(\left|\cos\left[\frac{\pi tk}{\sqrt{\tau}\mu}\right]\right|\sin\left[\frac{k\pi\varsigma}{\mu}\right]\right)+2\sum_{k=1}^{n}\left(\left|O\left[\frac{1}{k^1}\right]\right|\sin\left[\frac{k\pi\varsigma}{\mu}\right]\right)\right|\le M$$

The second series in the last expression converges according to Dirichlet's test; therefore, the sequence of its partial sums is limited. Let us estimate the first sum in the last expression:

$$\sum_{k=1}^{n}\left(\left|\cos\left[\frac{\pi tk}{\sqrt{\tau}\mu}\right]\right|\sin\left[\frac{k\pi\varsigma}{\mu}\right]\right)\le\left|\sum_{k=1}^{n}\left(\sin\left[\frac{k\pi\varsigma}{\mu}\right]\right)\right|$$

The last partial sum under the modulus sign is the Dirichlet kernel, which is bounded if $n\to\infty$. If the sequence of the partial sums (72) is bounded, then the series (71) converges, *QED*. □

References

1. Pop, E., Sinha, S., Goodson, K.E.: Heat generation and transport in nanometer scale transistors. Proc. IEEE **94**, 1587–1601 (2006)
2. Tong, X.C.: Development and Application of Advanced Thermal Management Materials. Springer, New York (2011)
3. Haque, M.A., Saif, M.T.A.: Thermo-mechanical properties of nano-scale freestanding aluminum films. Thin Solid Films **484**(1–2), 364–368 (2005)
4. Jou, D., Casas-Vazquez, J., Lebon, G.: Extended Irreversible Thermodynamics. Springer, Berlin (2010)
5. Cattaneo, C.: A form of heat conduction equation which eliminates the paradox of instantaneous propagation. Compte Rendus **247**, 431–433 (1958)
6. Vernotte, P.: Les paradoxes de la theorie continue de lequation de la chaleur. CR Acad. Sci. **246**(22), 3154–3155 (1958)
7. Sieniutycz, S.: The variational principles of classic type for non-coupled non-stationary irreversible transport processes with convective motion and relaxation. Int. J. Heat Mass Transf. **20**(11), 1221–1231 (1977)
8. Müller, I., Müller, W.H.: Fundamentals of Thermodynamics and Applications: with Historical Annotations and Many Citations from Avogadro to Zermelo. Springer, Berlin (2009)

9. Germain, P., Nguyen, Q.-S., Suquet, P.: Continuum thermodynamics. J. Appl. Mech. **50**, 1010–1020 (1983)
10. Prigogine, I.: Introduction to Thermodynamics of Irreversible Processes. Wiley, New York (1968)
11. Truesdell, C.: Rational Thermodynamics: A Course of Lectures on Selected Topics. McGraw-Hill, New York (1969)
12. Chandrasekharaiah, D.S.: Hyperbolic thermoelasticity: a review of recent literature. Appl. Mech. Rev. **51**(12), 705–729 (1998)
13. Wang, C.-C.: Stress relaxation and the principle of fading memory. Arch. Ration. Mech. Anal. **18**(2), 117–126 (1965)
14. Tzou, D.Y.: Macro-to-Microscale Heat Transfer. The Lagging Behaviour. Taylor and Francis, New York (1997)
15. Levanov, E.I., Sotskii, E.N.: Some properties of the heat-transfer process in a motionless medium, taking account of heat-flux relaxation. J. Eng. Phys. **50**(6), 733–740 (1986)
16. Magunov, A.N.: Laser thermometry of solids: state of the art and problems. Meas. Tech. **45**(2), 173–181 (2002)
17. Liu, Y., Mandelis, A.: Laser optical and photothermal thermometry of solids and thin films. Exp. Methods Phys. Sci. **42**, 297–336 (2009)
18. Novikov, N.A.: Hyperbolic equation of thermal conductivity. Solution of the direct and inverse problems for a semiinfinite bar. J. Eng. Phys. **35**(4), 1253–1257 (1978)
19. Baumeister, K.J., Hamill, T.D.: Hyperbolic heat conduction equation—a solution for the semi-infinite problem. ASME J. Heat Transf. **91**, 543–548 (1969)
20. Polyanin, A.D.: Handbook of Linear Partial Differential Equations for Engineers and Scientists. Chapman and Hall/CRC, Boca Raton (2001)
21. Lewandowska, M.: Hyperbolic heat conduction in the semi-infinite body with a time-dependent laser heat source. Heat Mass Transf. **37**, 333–342 (2001)
22. Lam, T.T.: Thermal propagation in solids due to surface laser pulsation and oscillation. Int. J. Therm. Sci. **49**, 1639–1648 (2010)
23. Isakovich, M.A.: Obshhaja akustika (General Acoustics, in Russ.). Nauka, Moscow (1973)
24. Doetsch, G.: Guide to the Applications of the Laplace and Z-Transforms. 2nd edn. Van Nostrand-Reinhold, London (1971)
25. Beaty, H.W., Fink, D.G. : Standard Handbook for Electrical Engineers. Mc Graw Hill, New Yourk (2012)
26. Nowacki, W.: Dynamic Problems of Thermoelasticity. Springer, Warsaw (1975)
27. Berber, S., Kwon, Y.K., Tomanek, D.: Unusually high thermal conductivity of carbon nanotubes. Phys. Rev. Lett. **84**(20), 4613–4616 (2000)
28. Mo, Z., Anderson, J., Liu, J.: Integrating nano carbontubes with microchannel cooler. In: Proceeding of the Sixth IEEE CPMT Conference on High Density Microsystem Design and Packaging and Component Failure Analysis HDP'04, pp. 373–376 (2004)
29. Debye, P.: Zur theorie der spezifischen wärmen. Ann. Phys. **344**(14), 789–839 (1912)
30. Matsunaga, R.H., Santos, I.: Measurement of the Thermal Relaxation Time in Agar-gelled Water. In: Proceedings of 34th Annual International Conference of the IEEE EMBS San Diego, California USA, pp. 5722–5725 (2012)
31. Kaminski, W.: Hyperbolic heat conduction equation for materials with a non-homogeneous inner structure. ASME J. Heat Transf. **112**, 555–560 (1990)
32. Mitra, K., Kumar, S., Vedavarz, A., Moallemi, M.K.: Experimental evidence of hyperbolic heat conduction in processed meat. ASME J. Heat Transf. **117**, 568–573 (1995)
33. Grabmann, A., Peters, F.: Experimental investigation of heat conduction in wet sand. Heat Mass Transf. **35**, 289–294 (1999)
34. Herwig, H., Beckert, K.: Experimental evidence about the controversy concerning Fourier or non-Fourier heat conduction in materials with a non-homogeneous inner structure. Heat Mass Transf. **36**, 387–392 (2000)
35. Roetzela, W., Putra, N., Das, S.K.: Experiment and analysis for non-Fourier conduction in materials with non-homogeneous inner structure. Int. J. Therm. Sci. **42**, 541–552 (2003)
36. Chester, M.: Second sound in solids. Phys. Rev. **131**, 2013–2015 (1963)